# Supplementary Information

## Cryo–EM structure of the ribosome–SecYE complex in the membrane environment

Jens Frauenfeld[1,2], James Gumbart[3], Eli O. van der Sluis[1,2], Soledad Funes[4], Marco Gartmann[1,2], Birgitta Beatrix[1,2], Thorsten Mielke[5], Otto Berninghausen[1,2], Thomas Becker[1,2], Klaus Schulten[3] and Roland Beckmann[1,2, #]

[1] *Gene Center, Department for Biochemistry, University of Munich, Feodor–Lynen–Str. 25, 81377 Munich, Germany*

[2] *Munich Center For Integrated Protein Science (CIPSM), Department of Chemistry and Biochemistry, Butenandtstr. 5–13, 81377 Munich, Germany*

[3] *Department of Physics, Beckman Institute, University of Illinois at Urbana–Champaign, Urbana, IL, 61801, USA*

[4] *Departamento de Genética Molecular, Instituto de Fisiología Celular, Circuito Exterior S/N, Ciudad Universitaria, Universidad Nacional Autónoma de México, Mexico, D.F., 04510, Mexico*

[5] *Ultrastrukturnetzwerk, Max Planck Institute for Molecular Genetics, Ihnestr. 63–73, 14195 Berlin, Institut für Medizinische Physik und Biophysik, Charite–Universitätsmedizin Berlin, Ziegelstrasse 5–9, 10117–Berlin, Germany*

[#] *Corresponding author*

Roland Beckmann: Email: beckmann@lmb.uni-muenchen.de

Tel: +49 89 2180 76900

Fax: +49 89 2180 76945

## Supplementary Methods

### MDFF

MDFF is a method to flexibly fit atomic models into cryo-EM density maps while simultaneously preserving the stereochemical accuracy of model[1,2]. In MDFF, the atomic model is simulated using molecular dynamics in the presence of the cryo-EM density map, represented through an additional potential in the simulation. From this potential, forces proportional to the gradient of the cryo-EM density are derived that then drive atoms into high-density regions of the map. In addition, restraints are applied to maintain the secondary structure of protein and RNA molecules, which otherwise would distort or break under the forces required for fitting. Fitting of the 70S proceeded in stages using an approach employed previously[1,3,4]. A total simulation time of 3.5 ns was used to fit the ribosome.

### Simulations

All MD simulations, including MDFF, were carried out using NAMD 2.7b1[5] and the CHARMM27 force field with CMAP corrections[6-8]. Simulation protocols, including multiple time-stepping and particle mesh Ewald, are identical to those used in Gumbart et al.[3]. After completion of modeling and MDFF, the resulting ribosome-Nanodisc model was used for further equilibrium simulations. Water and ions were added in an iterative procedure using VMD[9]. To reduce simulation complexity and to focus on the interactions between the ribosome and SecYE and Nanodisc, the ribosome and nascent chain were truncated just downstream of the L4/L22 constriction point. Any ribosomal backbone atoms within 5 Å of the truncation point


Nature Structural & Molecular Biology: doi:10.1038/nsmb.2026

were constrained. At the point of closest approach, SecYE was at least 25 Å away from the truncation point. While previous simulations of the ribosome-SecY complex required 2.7 million atoms[3], simulation of the truncated ribosome-Nanodisc complex required only 400,000 atoms.

Equilibration of the system occurred in stages. First, only the lipid tails were allowed to move, permitting them to "melt", for 0.25 ns. Next, water and sidechains were released for an additional 2.25 ns. For the next 1.5 ns, only the encircling Apo A-1 proteins of the Nanodisc were constrained; the secondary structure of all proteins and RNA was also enforced during this time, and for a further 2 ns. Finally, after 6 ns of total simulation time, all restraints were released. At all times, a constant temperature of 310 K and a constant pressure of 1 atm were maintained.

**Figures**

Densities for the large and small ribosomal subunit, the P-site tRNA, the nascent FtsQ-chain, the *E. coli* SecYE and the Nanodisc-Lipid-Bilayer were isolated using the color zone function of Chimera[10]. A lower contour level of the ligand densities for surface representation was applied for some figures. This indicates that ligand densities are partially flexible or still under-represented because of incomplete removal of ligand-free ribosomal particles from the final particle subset. Supplemental Fig. 1a shows the entire electron density filtered at different resolutions using only one contour level for all parts.


Nature Structural & Molecular Biology: doi:10.1038/nsmb.2026

## Supplementary Figure Legends

### Supplementary Fig. 1: Raw data, effect of resolution on TM helices

**(a)** The complete 70S-RNC-Nd-SecYEG density is shown, filtered at different frequencies ranging from 6-10 Å, as indicated.

**(b)** Close-up of the 50S-Nd-SecYEG density, side view cut perpendicular to the plane of the membrane to show the lateral gate of SecY, filtered from 6-10 Å, as indicated. Two layers of density are visible (upper membrane interface, UMI and lower membrane interface, LMI), separated by a region of lower density (hydrophobic core, HC), containing rod-like features.

**(c)** Close-ups of the Nanodisc-density, showing different views with the fitted models of SecY (orange), SecE (purple), the signal anchor (green) and the electron density represented in grey mesh.

### Supplementary Figure 2: Canonical binding of PCCs to ribosomes

**(a)** Close-up on the interaction of cytosolic loop L8/9 of the mammalian Sec61 complex (red, PDB: 2WWB[11]) with the eukaryotic 80S ribosome

**(b)** Close-up on the interaction of cytosolic loop L8/9 of a mixed model of the archeal SecYEβ complex with L6/7 and L8/9 replaced by a model of the corresponding *E.coli* SecY loops (purple, PDB: 3BO0[12])

**(c)** Close-up on the interaction of cytosolic loop L8/9 of the *E.coli* SecYEG complex (orange) with the prokaryotic 70S RNC and an inserted signal anchor


Nature Structural & Molecular Biology: doi:10.1038/nsmb.2026

**(d)** Close-up of the map filtered at 6-7 Å showing the interaction of cytosolic loop L8/9 of the *E.coli* SecYEG complex with the fitted models of the *E.coli* SecYEG complex (orange) with the prokaryotic 70S RNC and an inserted signal anchor

**(e)** as in (d), but rotated around 180°

**Supplementary Figure 3: Fitting of SecY structures into the cryo-EM density and comparison with the 2D crystal structure of the *E. coli* SecYEG complex**

**(a)** Close-up of the SecY density, side view cut perpendicular to the plane of the membrane to show SecY TM helices 6, 8, 9 with fitted X-ray structures of SecY *M. janaschii* (blue, left), *T. maritima* (yellow, middle) and our *E. coli* model (orange, right).

**(b)** Close-up of the SecY density, side view cut perpendicular to the plane of the membrane to show the lateral gate with SecY TM helices 2, 3, 7, 8, 9 with fitted X-ray structures of SecY *M. janaschii* (blue, left), *T. maritima* (yellow, middle) and our current *E. coli* model (orange, right).

**(c)** Cytosolic view of the electron density projection map of the 2D crystal structure of the *E. coli* SecYEG complex with the fitted X-ray structure of the SecYEβ from *M. jannaschii*[13]. SecY TM helices in red and labelled in green, SecE C-terminal helix in grey (figure adapted from ref#13).

The position of the two additional N-terminal helices of *E. coli* SecE is labelled in purple, Secβ in grey.


Nature Structural & Molecular Biology: doi:10.1038/nsmb.2026

**(d)** Cytosolic view of the electron density map of the cryo-EM structure of the open *E. coli* SecYEG complex. SecY TM helices in orange, SecE TM helices in purple, signal anchor (SA) in green. Note the slightly outward shifted position of the SecE N-terminal density compared to its position in the 2D-crystal map. The position of the SecG TM helices (red) is according to an alignment of the X-ray structure of the SecYEG complex from *T. maritima* on our *E. coli* model.

**(e)** as in (d), with the aligned X-ray structure of the SecYEG complex from *T. maritima* (red) on our *E. coli* model.

**Supplementary Figure 4: RMSD values of SecYE and of the signal anchor relative to SecYE.**

The root-mean-square deviation (RMSD) over time is presented for (a) the backbone of SecYE and (b) that of the signal anchor. In both cases, RMSD was calculated after first performing a least-squares fit of SecYE over all frames of the simulation trajectory. Data for the initial 2.5 ns of the simulation in which the proteins were restrained are not shown.

**Supplementary Figure 5: Formation of H-bonds during simulation.**

Hydrogen bonds formed between different components of the simulation over time are shown. (a,b) H-bonds between the ribosome and (a) SecY and (b) SecE. (c,d) H-bonds between SecY and (c) the nascent chain and (d) the signal anchor. The solid black line denotes a running average of the full data in light grey. Only data from the last 10 ns of the simulation, i.e., the completely unrestrained portion, are shown. H-


Nature Structural & Molecular Biology: doi:10.1038/nsmb.2026

bonds were counted when the distance between the hydrogen donor and the acceptor was within 3.5 Å and the angle formed by the donor, hydrogen, and acceptor was greater than 145°.

**Supplementary Figure 6: Surface representation of the all-atom model of a 70S-RNC-Nd-SecYEG complex**

**(a)** Surface representation of the all-atom model of a 70S-RNC-Nd-SecYE complex that was used for the free MD simulation, coloured as in Fig. 1. Phospholipid headgroups are red (oxygen) and blue (nitrogen). Right: close-up of the isolated SecYE complex in the same position within the Nanodisc of the left panel.

**(b)** as in (a), but rotated 90° around the y-axis.

**(c)** as in (b), but rotated 90° around the y-axis.

**Supplementary Figure 7: Analysis of ribosomal proteins L22, L23, L24**

Comparison of X-ray structures and cryo-EM densities of an inactive ribosome (PDB: 2I2V) vs. MDFF-models and cryo-EM densities of an active ribosome.

**(a)** Conformation of L22. Left, isolated density of L22 in an inactive ribosome with the fitted X-ray structure of L22 of an inactive ribosome (dark grey). Middle-left, isolated density of L22 in active ribosome with the fitted X-ray structure of L22 of an inactive ribosome (dark grey). Middle-right, isolated density of L22 in an active ribosome with a MDFF-model of L22 of an active ribosome (light blue). Right, overlay of the X-ray structure of the inactive L22 with the MDFF-model of L22.


Nature Structural & Molecular Biology: doi:10.1038/nsmb.2026

**(b)** Conformation of L23, side view as in Fig.4b. Left, isolated density of L23 in an inactive ribosome with the fitted X-ray structure of L23 of an inactive ribosome (dark grey). Middle-left, isolated density of L23 in active ribosome with the fitted X-ray structure of L23 of an inactive ribosome (dark grey). Middle-right, isolated density of L23 in an active ribosome with a MDFF-model of L23 of an active ribosome (light blue). Right, overlay of the X-ray structure of the inactive L23 with the MDFF-model of L23.

**(c)** Conformation of L24, side view as in Fig.4c. Left, isolated density of L24 in an inactive ribosome with the fitted X-ray structure of L24 of an inactive ribosome (dark grey). Middle-left, isolated density of L24 in active ribosome with the fitted X-ray structure of L24 of an inactive ribosome (dark grey). Middle-right, isolated density of L24 in an active ribosome with a MDFF-model of L24 of an active ribosome (light blue). Right, overlay of the X-ray structure of the inactive L24 with the MDFF-model of L24.

**Supplementary Figure 8: Comparison of L6/7 conformation within the ribosomal tunnel**

Close-up of a section through the ribosomal exit tunnel with fitted models of L6/7 of SecY.

**(a)** A model for an inactive, monomeric SecY bound to a non-translating ribosome (purple, PDB: 3BO0) was fitted according to the position of ribosomal RNA and superimposed to our model of the translating ribosome with the nascent chain (green). In that position, L6/7 of the inactive SecY would prevent the exit of the nascent chain.


Nature Structural & Molecular Biology: doi:10.1038/nsmb.2026

Upper panel: side view, lower panel: view from the inside of the ribosomal tunnel towards the ribosomal exit

**(b)** as in (a), but with a model for an inactive, monomeric SecY with an alternate L6/7 conformation binding to a non-translating ribosome (ruby, PDB: 3BO1). Also in this position, the exit of the nascent chain is hindered by L6/7 of the inactive SecY.

**(c)** view as in (a). The model for the translating ribosome bound to an open SecY (orange) within a membrane environment. L6/7 reaches up along the wall of the ribosomal tunnel and contacts both, the nascent chain and L23. The position of L6/7 within the ribosomal exit tunnel of the hybrid complex allows the exit of the nascent chain

**(d)** view as in (a), but with a model for the mammalian Sec61 complex bound to a translating wheat germ ribosome (red, PDB: 2WWB), fitted according to the position of ribosomal RNA and superimposed to our model of the translating ribosome with the nascent chain (green). The position of L6/7 within the ribosomal exit tunnel of the hybrid complex allows the exit of the nascent chain.

**(e)** Close-up of the density showing the interaction of L6/7 with the nascent chain in the ribosomal exit tunnel with the fitted models for SecY, 50S subunit and the nascent chain

**Supplementary Figure 9: Conformational changes and opening of SecYE.**

**(a)** View of the lateral gate of the PCC. Comparison of the membrane-embedded, open ribosome-bound SecYE (orange, purple) with SecYE from the *T. maritima* SecA-SecYEG complex (grey). Loop movements are indicated with round arrows,


Nature Structural & Molecular Biology: doi:10.1038/nsmb.2026

helix movements are indicated with small black arrows. SA in green, the NC has been omitted for better clarity.

**(b)** as in (a), but viewed from the cytoplasmic side with the NC in green.

**(c)** Comparison of SecY structures in different conformations, viewed from the cytoplasmic side. Left, structure of the closed, detergent-solubilised SecY from *M. janaschii* (PDB: 1RHZ). Middle left, structure of the pre-open, detergent-solubilised SecY from *T. maritima*. Middle right, model of the open, membrane-embedded SecY from *E. coli*. Right, model of the open, membrane-embedded SecY from *E.coli* with a SA helix within the lateral gate

**(d)** as in c, but view of the lateral gate

**Supplementary Figure 10: Horizontal sections of Nd-SecYEG and corresponding models**

Three consecutive horizontal sections, sliced within the plane of the membrane in the hydrophobic core of the lipid bilayer, as indicated (1, upper; 2, middle; 3, lower).

**(a)** Sections through the experimental map at 7-8 Å with the fitted model for Nd-SecYEG and the signal anchor. Charged lipid headgroups are visible within the slices. The likely position of the SecG TM helices (marked) in the density is according to the X-ray structure of the SecYEG complex from *T. maritima*.

**(b)** Sections through a density based on the molecular model for SecYE/SA within the Nanodisc at 7-8 Å. Additional density from charged lipid headgroups are visible, similar to the appearance of the experimental map. Since the model does not include


Nature Structural & Molecular Biology: doi:10.1038/nsmb.2026

SecG, the density does not display rod-like features in the position where SecG is expected, in contrast to the experimental map.

**(c)** Sections through a density based on the molecular model for SecYE/SA without the Nanodisc (no lipids) at 7-8 Å. No additional density from charged lipid headgroups is visible.

**(d)** Sections through a density based on the X-ray structure of the SecYEG complex from *T. maritima* at 7-8 Å.

**Supplementary Figure 11: Plot of ribosome-lipid contact area during simulation.**

The surface area of interaction (measured in $Å^2$) vs. time between the membrane and (a) the entire ribosome, (b) L23, and (c) L24 is shown. The blue lines at 2.5 ns and 6 ns denote the different stages of equilibration, noted in part (a) and in the MD Simulations section of the Methods.

**Supplementary Figure 12: Comparison of the position of the signal anchor with respect to the ribosome in (i) a SRP bound state and (ii) the PCC-inserted state**

**(a)** Close-up of the ribosomal exit site. A molecular model of SRP bound to a translating ribosome with a signal anchor[14] (PDB: 2j28). Note the orientation of the signal anchor with respect to ribosomal rRNA H59.

**(b)** Same view as in (a), but now with the molecular model of the PCC-inserted signal anchor. Note the orientation of the signal anchor with respect to H59.

**(c)** As in (a), rotated 90°

**(d)** As in (b), rotated 90°


Nature Structural & Molecular Biology: doi:10.1038/nsmb.2026

**Supplementary Table 1: Cross-correlation coefficients**

Cross-correlation coefficients for different structures. An isolated map of the transmembrane region of SecYE and the signal anchor/nascent chain filtered at 7-8 Å was used for all calculations. Simulated maps were generated at a resolution of 7.5 Å. "Initial" and "final" refer to pre- and post-MDFF states, respectively. For the rotated structure, SecY (or SecYE) and nascent chain were rotated about SecY's central axis 180˚.

**Supplementary Table 2: Ribosome-SecY interactions.**

Interactions between residues in the ribosome and in SecY. Specific residue-residue interactions were calculated over 0.5 ns of equilibration in which the backbone of all protein and RNA was restrained; thus, the interactions listed represent the fitted structure only. The criteria for H-bonds is given in Supplementary Figure 10; hydrophobic/hydrophilic interactions were counted when hydrophobic/hydrophilic heavy (non-hydrogen) atoms came within 4.0 Å of each other, respectively. Interactions were only counted when they appeared in at least 10% of frames, i.e., 50 out of the 500 frames taken every ps in the 0.5 ns simulation. If they appeared in between 10% and 20% of frames, they are denoted as weak.

**Supplementary Table 3: Ribosome–SecE interactions.**

Interactions between the ribosome and SecE. See the caption of Supplementary Table 1 for a description.

**Supplementary Table 4: NC-ribosome-SecY interactions.**

Interactions between the nascent chain and SecY and the ribosome. See the caption of Supplementary Table 1 for a description.


Nature Structural & Molecular Biology: doi:10.1038/nsmb.2026

**Supplementary Table 5: NC-SecY interactions.**

Interactions between the nascent chain and SecY. See the caption of Supplementary Table 1 for a description.

**Supplementary Table 6: SA-SecY interactions.**

Interactions between the SecY and the signal anchor. See the caption of Supplementary Table 1 for a description.

**Supplementary Table 7: Interactions between H59 and lipids**

Figure: Interactions between H59 of the ribosome and lipids. (a) Ribosome-SecY-nanodisc system. H59 is indicated in red. (b) Direct hydrogen bonding between a backbone phosphate of H59 and a PE lipid molecule. (c) $Mg^{2+}$-bridged interaction between the phosphates of H59 and a PE lipid molecule. (d) $Mg^{2+}$-bridged interaction between a phosphate of H59 and the head group of a PG lipid molecule.

Table: Interactions between H59 of the ribosomal 23S RNA and lipids during free equilibration of ribosome-SecYE-nanodisc system (10-ns simulation). Interactions are classified into three types: hydrogen bonds, hydrophilic and ion-bridging. An ion-bridging interaction is counted when a $Mg^{2+}$ ion is less than 5 Å from negatively charged atoms of both an RNA base and a lipid headgroup. The interaction is considered stable when it persists for at least 200 ps. Interactions primarily involved the RNA backbone on one side and the lipid phosphate or the $NH^{+3}$ group of PE on the other side.


Nature Structural & Molecular Biology: doi:10.1038/nsmb.2026

## Supplementary References


1 Trabuco, L.G., Villa, E., Mitra, K., Frank, J., & Schulten, K., Flexible fitting of atomic structures into electron microscopy maps using molecular dynamics. *Structure* 16 (5), 673-683 (2008).

2 Trabuco, L.G., Villa, E., Schreiner, E., Harrison, C.B., & Schulten, K., Molecular dynamics flexible fitting: a practical guide to combine cryo-electron microscopy and X-ray crystallography. *Methods* 49 (2), 174-180 (2009).

3 Gumbart, J., Trabuco, L.G., Schreiner, E., Villa, E., & Schulten, K., Regulation of the protein-conducting channel by a bound ribosome. *Structure* 17 (11), 1453-1464 (2009).

4 Villa, E. *et al.*, Ribosome-induced changes in elongation factor Tu conformation control GTP hydrolysis. *Proc Natl Acad Sci U S A* 106 (4), 1063-1068 (2009).

5 Phillips, J.C. *et al.*, Scalable molecular dynamics with NAMD. *J Comput Chem* 26 (16), 1781-1802 (2005).

6 MacKerell, A.D. *et al.*, All-Atom Empirical Potential for Molecular Modeling and Dynamics Studies of Proteins,Ä†. *The Journal of Physical Chemistry B* 102 (18), 3586-3616 (1998).

7 Foloppe, N., Mackerell, A., & Jr, All-atom empirical force field for nucleic acids: I. Parameter optimization based on small molecule and condensed phase macromolecular target data. *Journal of Computational Chemistry* 21 (2), 86-104 (2000).

8 Mackerell, A.D., Jr., Feig, M., & Brooks, C.L., 3rd, Extending the treatment of backbone energetics in protein force fields: limitations of gas-phase quantum mechanics in reproducing protein conformational distributions in molecular dynamics simulations. *J Comput Chem* 25 (11), 1400-1415 (2004).

9 Humphrey, W., Dalke, A., & Schulten, K., VMD: visual molecular dynamics. *J Mol Graph* 14 (1), 33-38, 27-38 (1996).

10 Pettersen, E.F. *et al.*, UCSF Chimera--a visualization system for exploratory research and analysis. *J Comput Chem* 25 (13), 1605-1612. (2004).

11 Becker, T. *et al.*, Structure of Monomeric Yeast and Mammalian Sec61 Complexes Interacting with the Translating Ribosome. *Science* (2009).

12 Menetret, J.-F. *et al.*, Ribosome Binding of a Single Copy of the SecY Complex: Implications for Protein Translocation. *Molecular Cell* 28 (6), 1083-1092 (2007).

13 Collinson, I., The structure of the bacterial protein translocation complex SecYEG. *Biochem Soc Trans* 33 (Pt 6), 1225-1230 (2005).

14 Halic, M. *et al.*, Following the signal sequence from ribosomal tunnel exit to signal recognition particle. *Nature* 444 (7118), 507-511 (2006).



Nature Structural & Molecular Biology: doi:10.1038/nsmb.2026

# Supplementary Figure 1

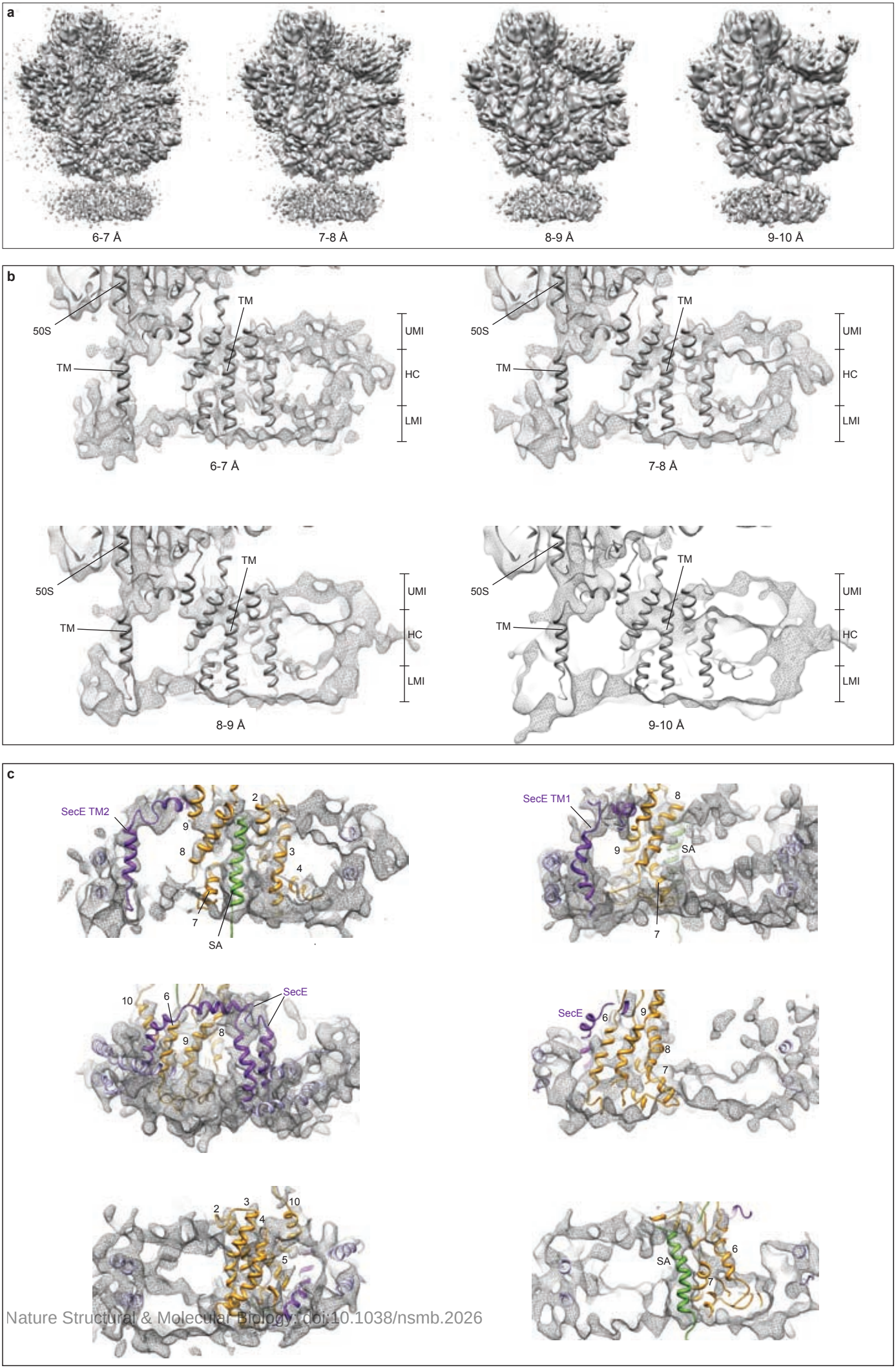


Nature Structural & Molecular Biology: doi:10.1038/nsmb.2026

Supplementary Figure 2

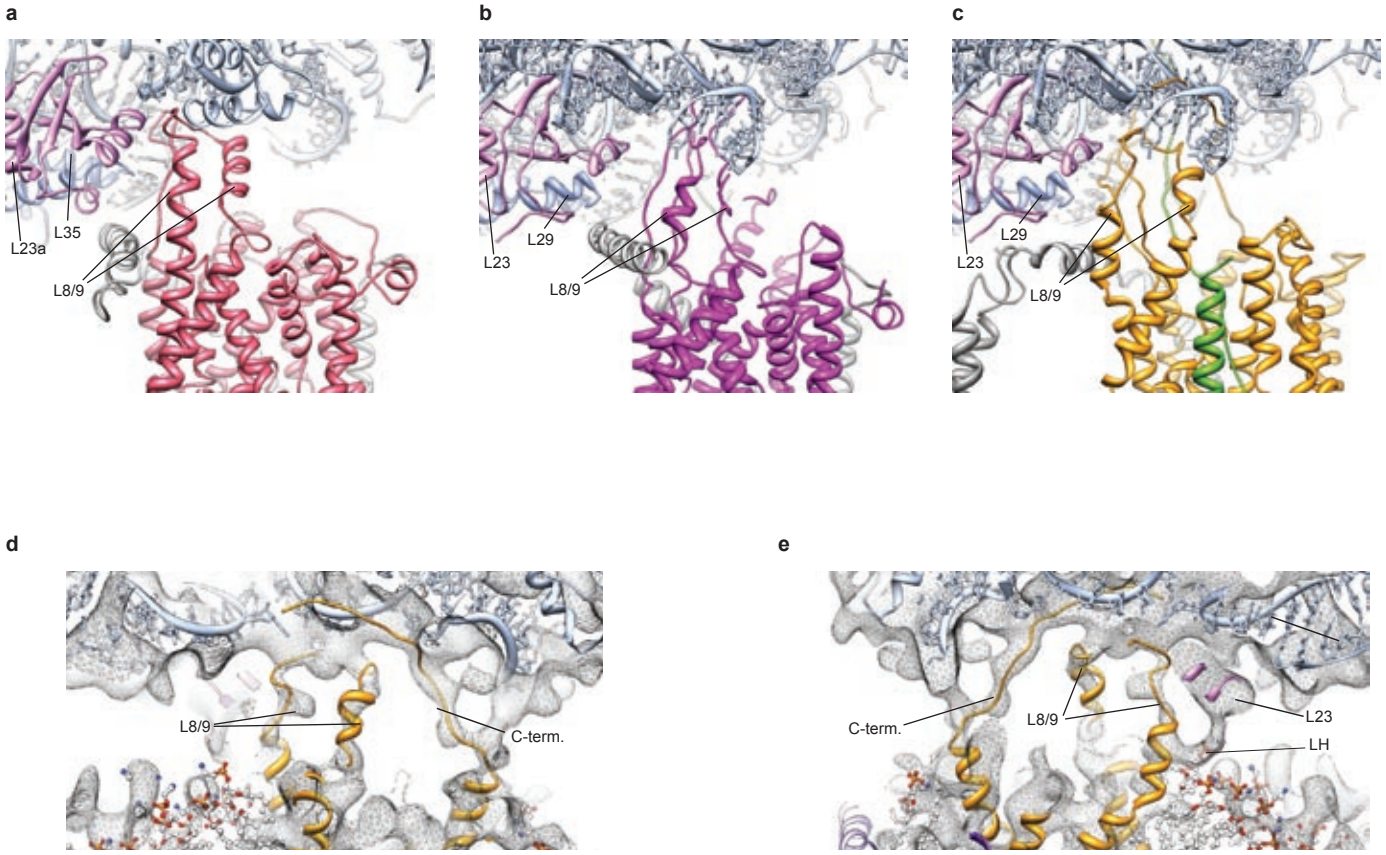

# Supplementary Figure 3

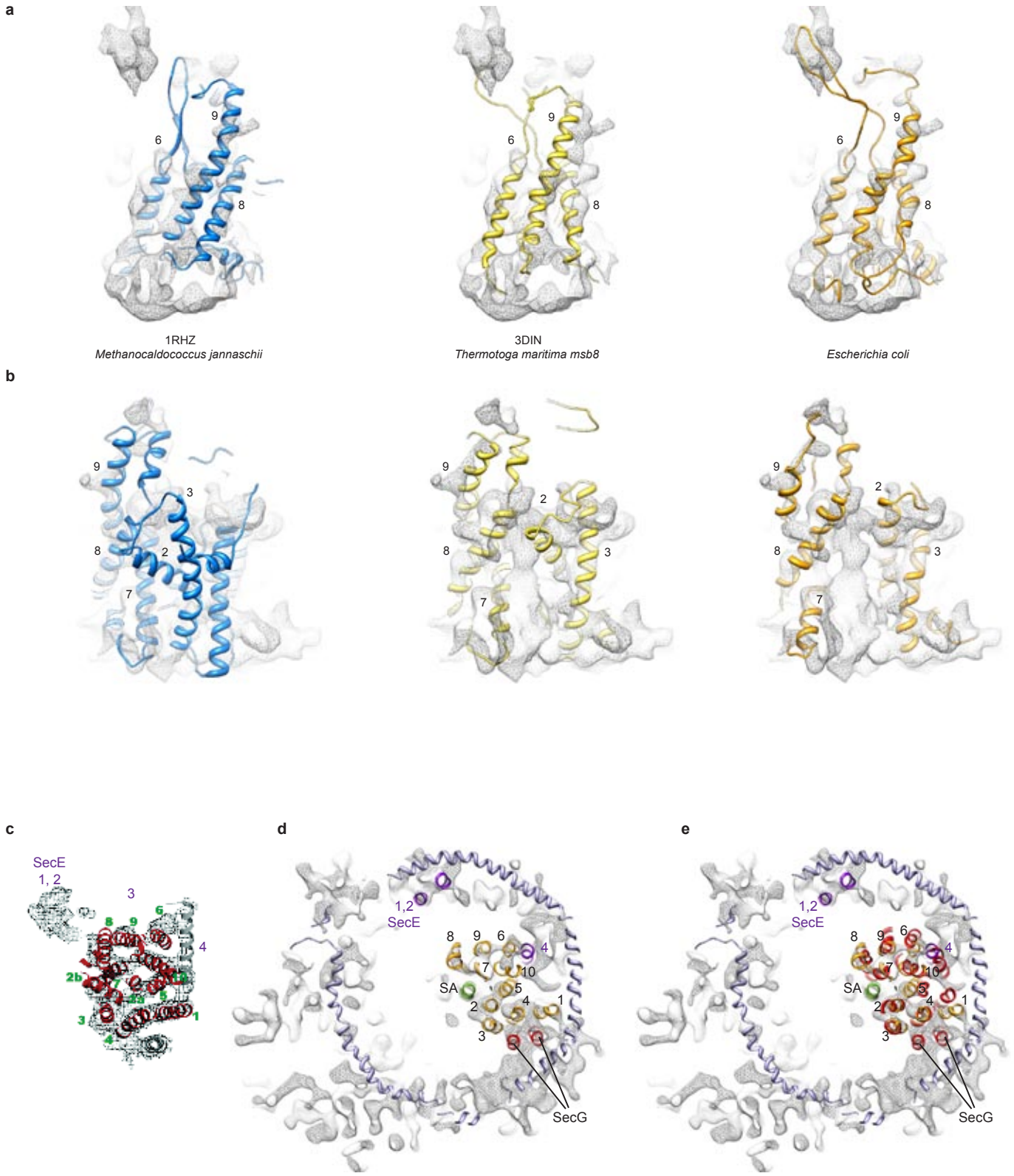

Supplementary Figure 4

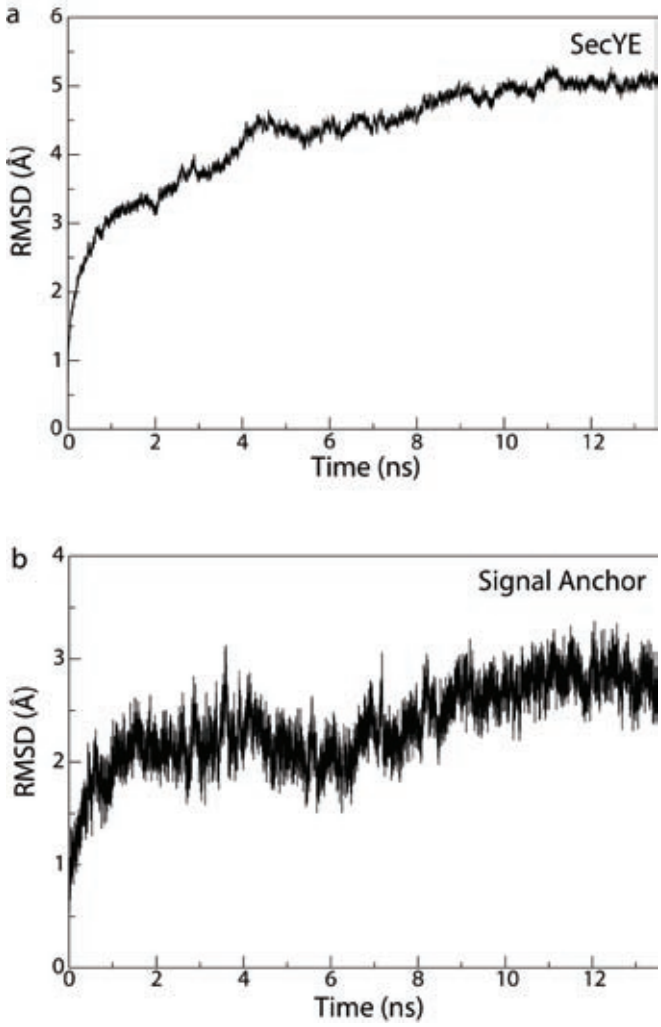

Supplementary Figure 5

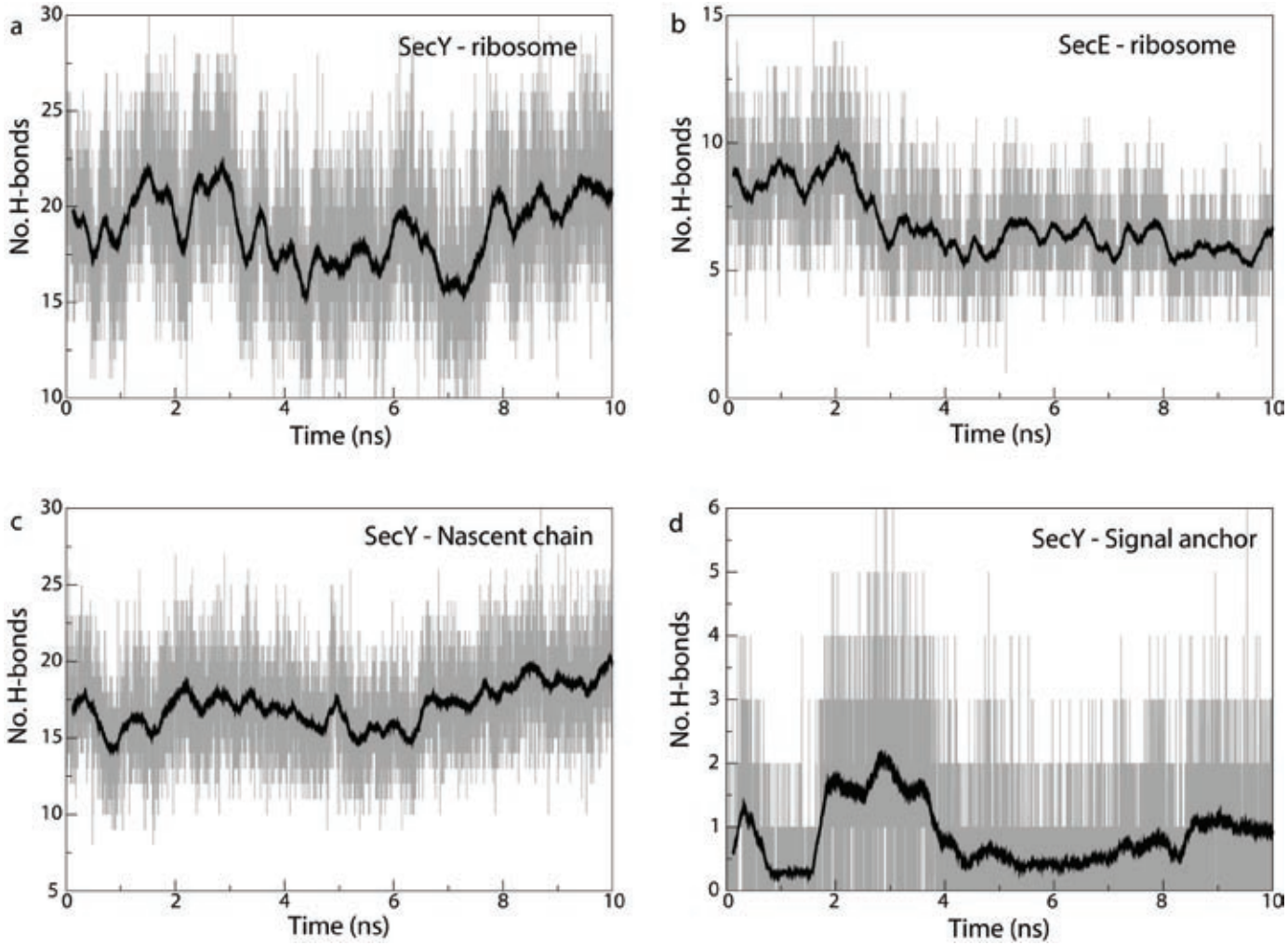

Supplementary Figure 6

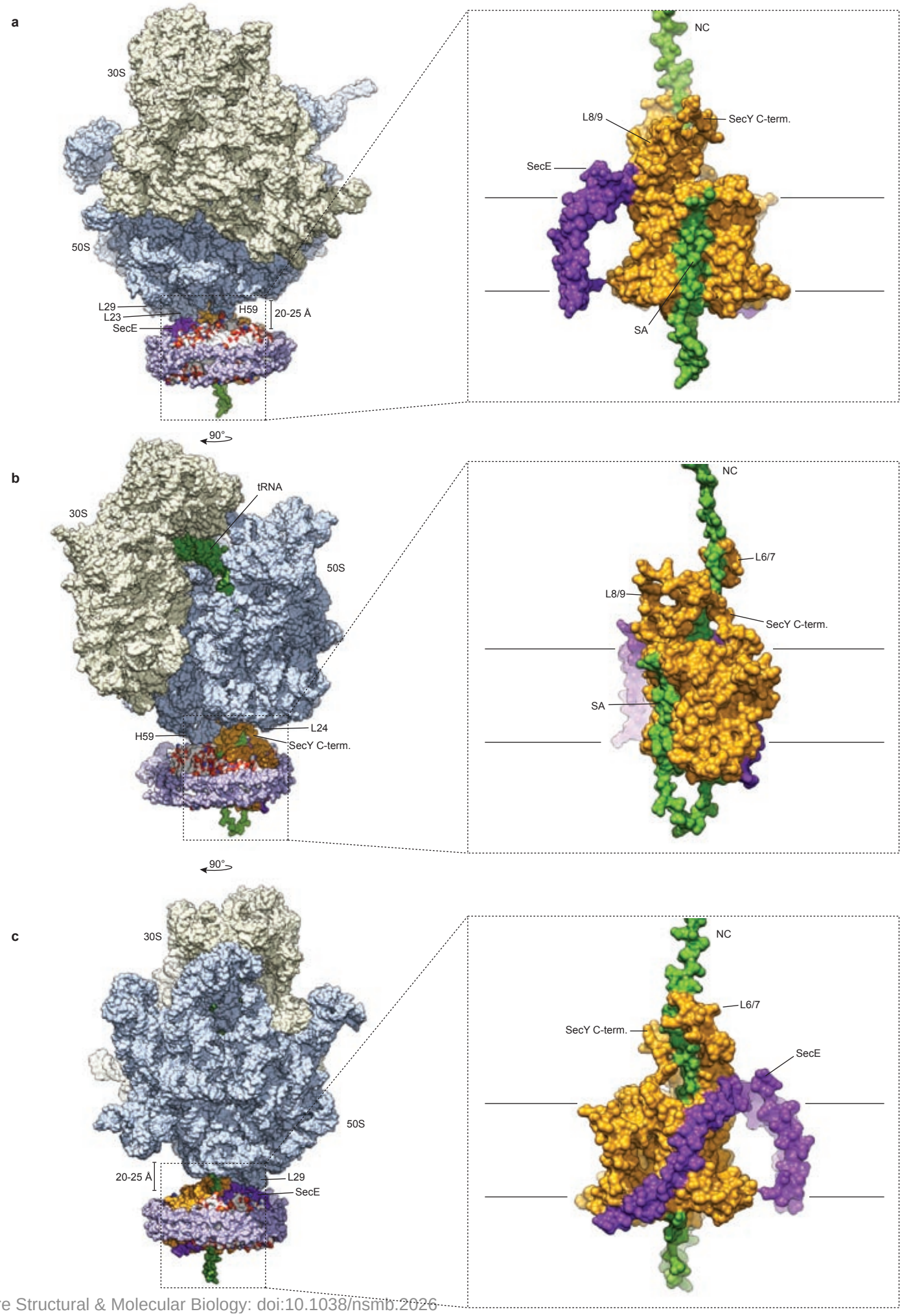

Supplementary Figure 7

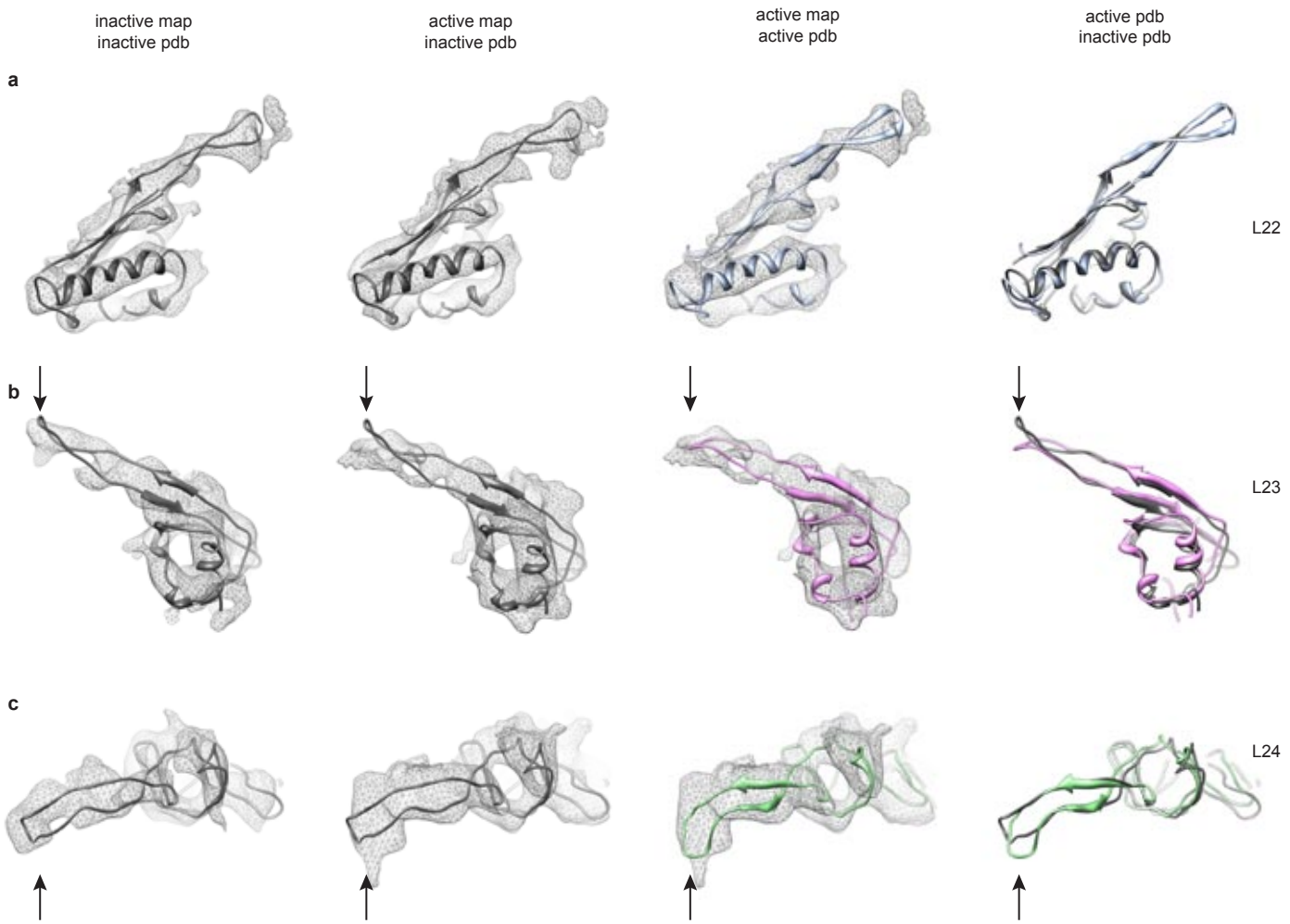

# Supplementary Figure 8

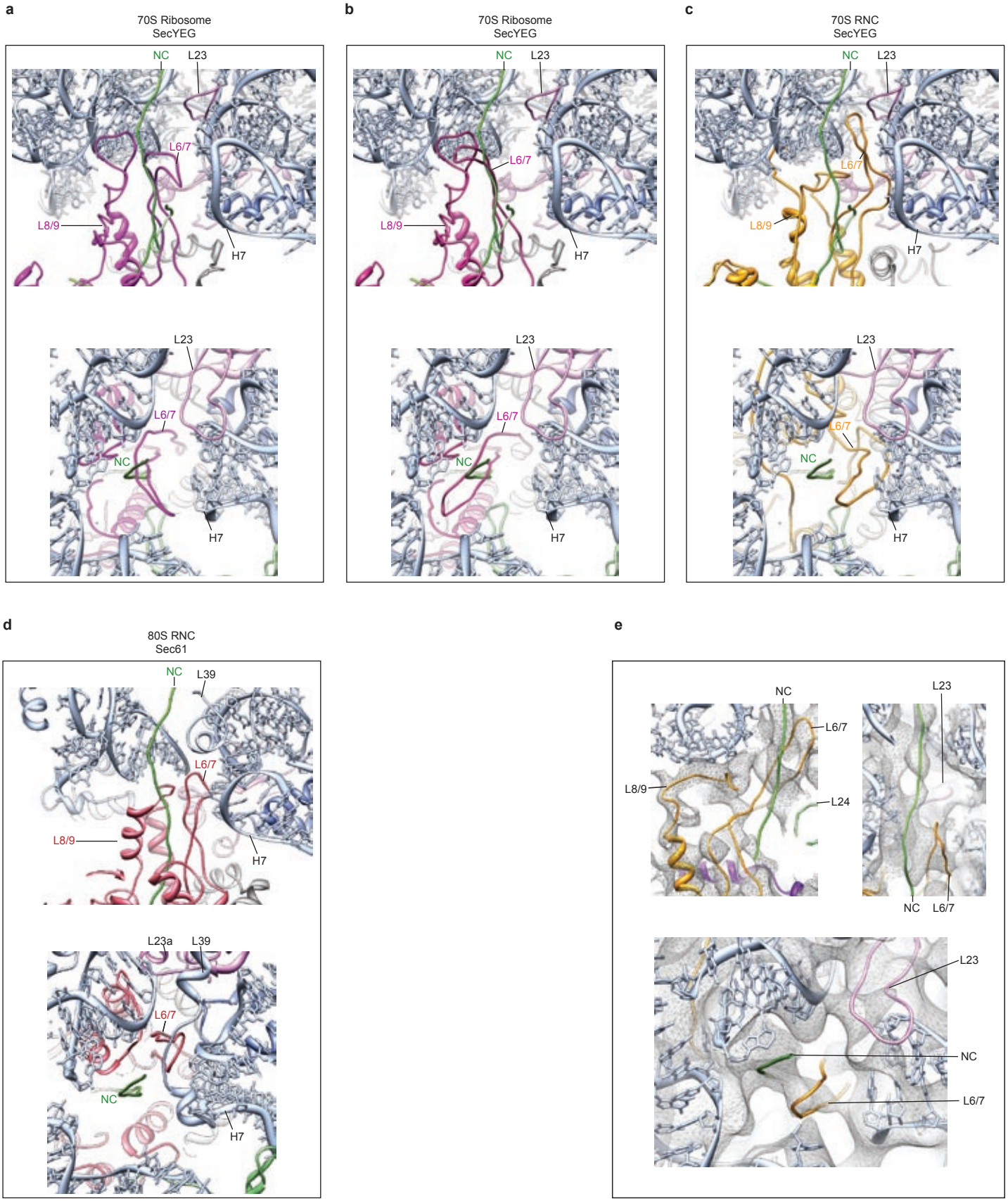

Supplementary Figure 9

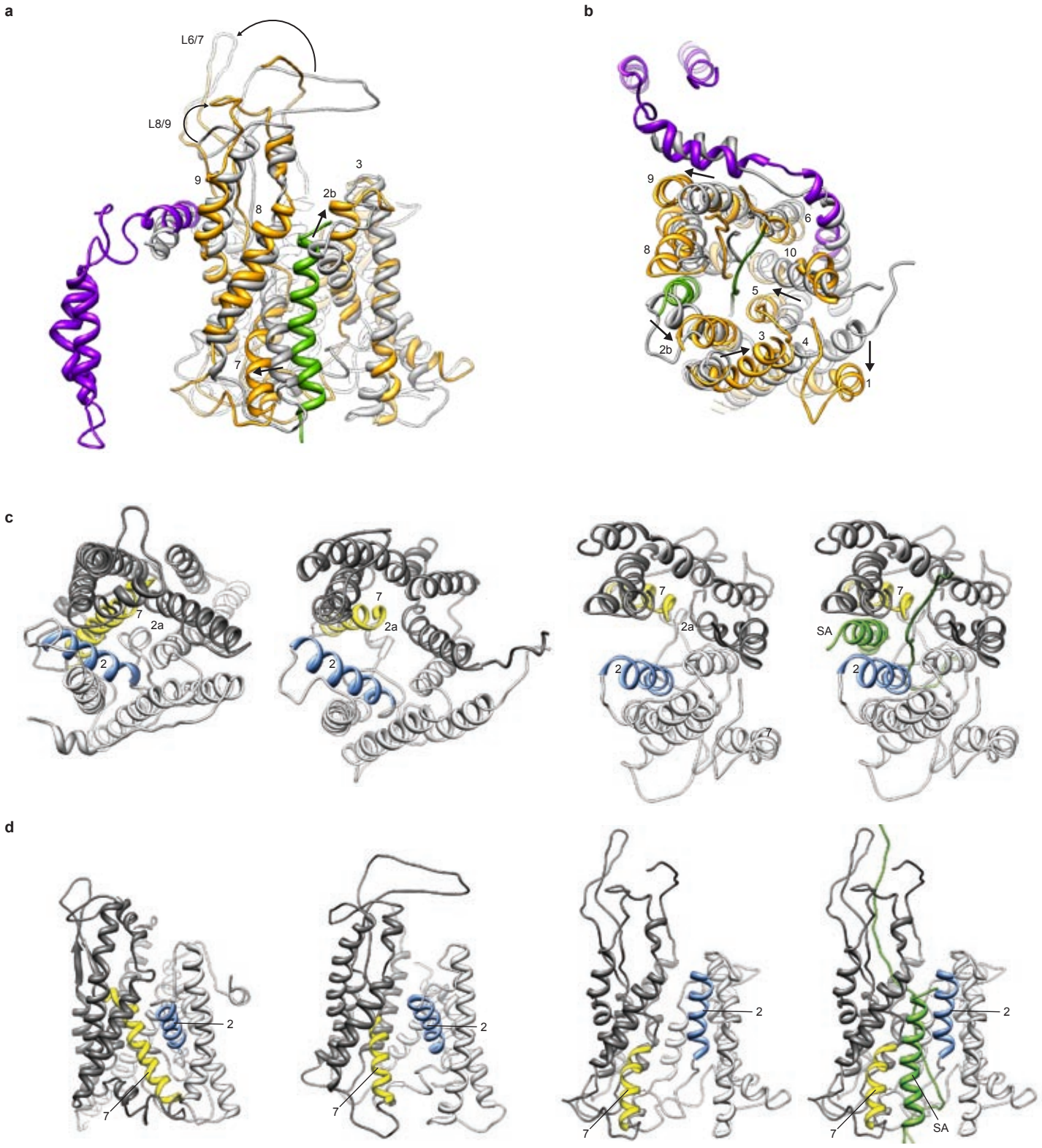

Supplementary Figure 10

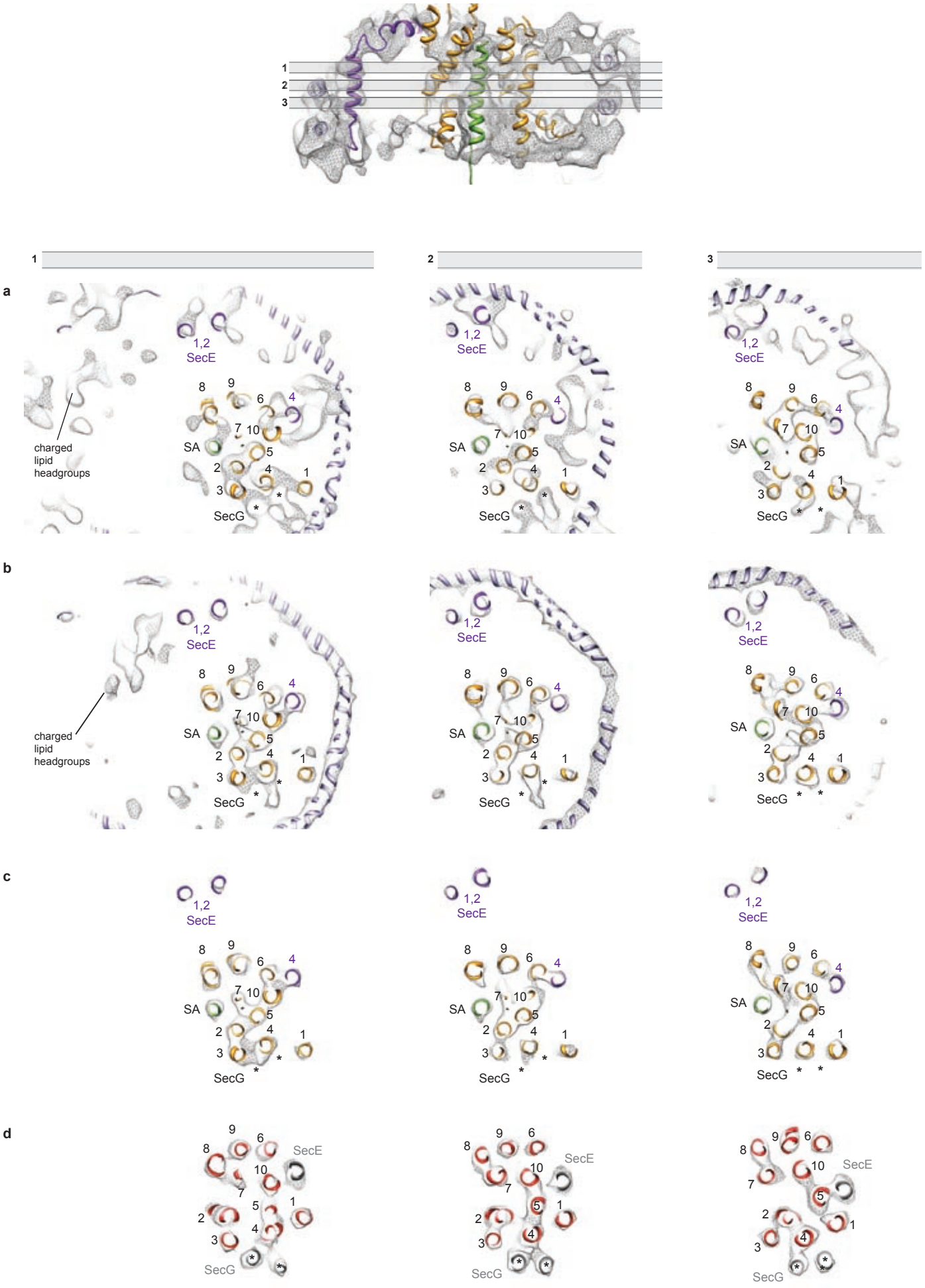

Supplementary Figure 11

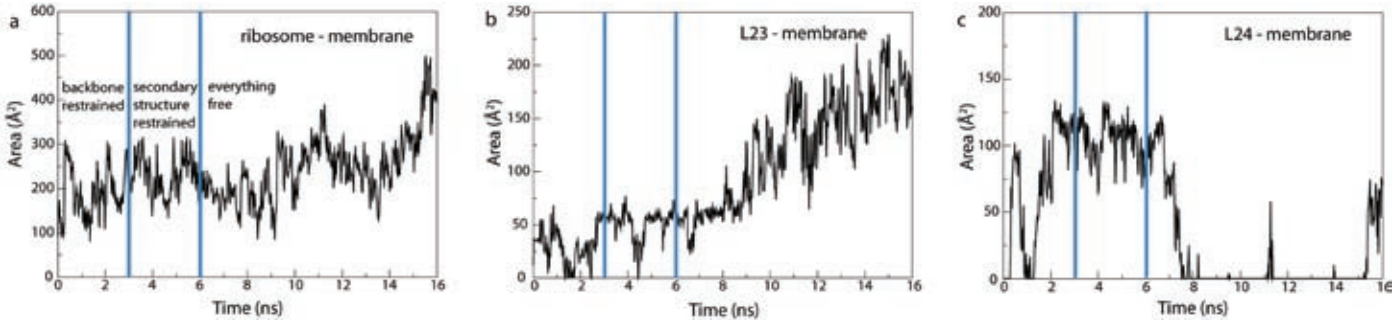

# Supplementary Figure 12

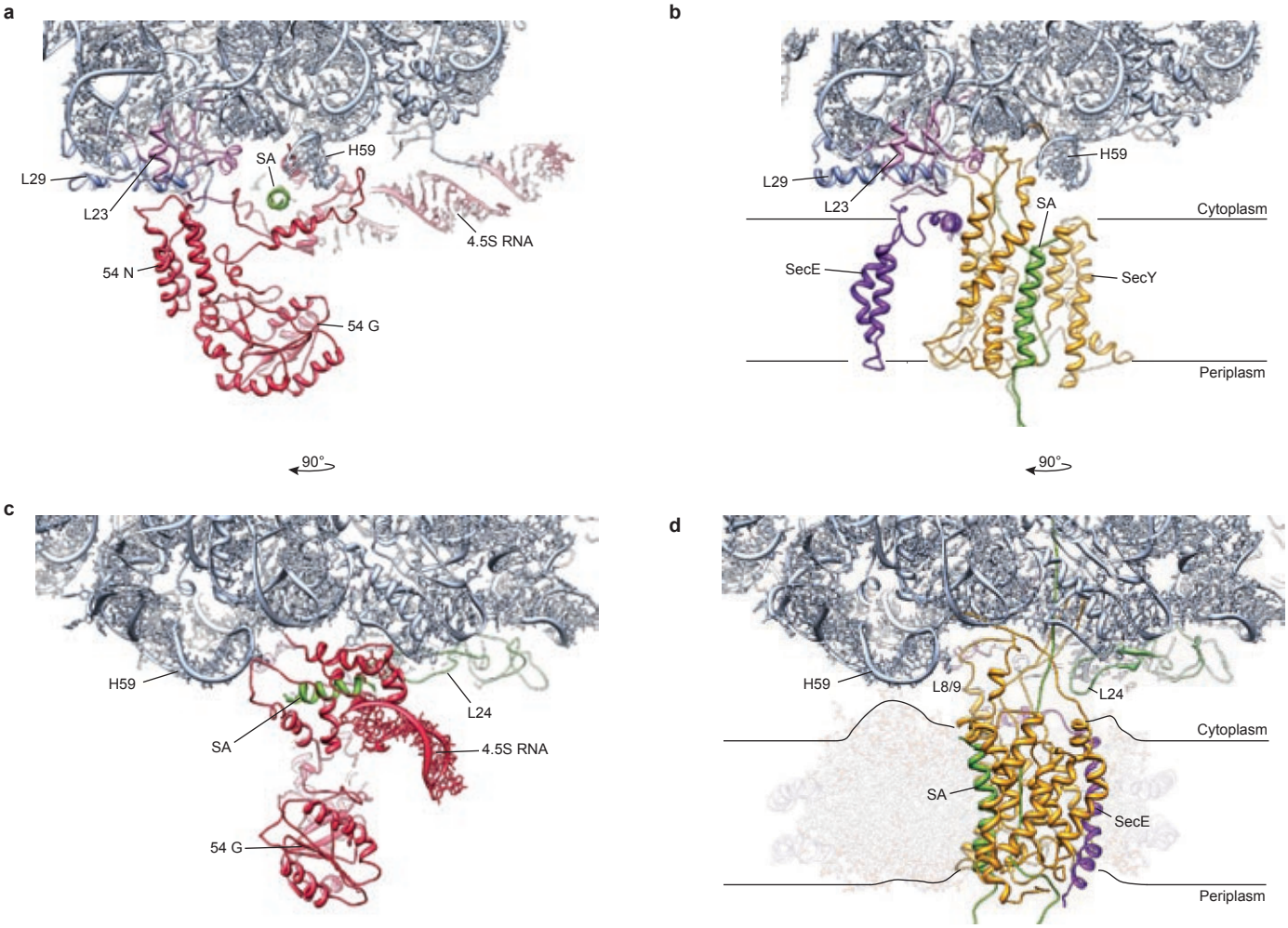

Supplementary Table 1: Cross-correlation coefficients

| Structure | Cross-correlation coeff. |
|---|---|
| SecY/SA (initial) | 0.54 |
| SecY/SA (final) | 0.65 |
| SecY/SA (rotated 180°) | 0.44 |
| 1RHZ (SecY only) | 0.39 |
| 3DIN (SecY only) | 0.48 |

| Structure | Cross-correlation coeff. |
|---|---|
| SecYE/SA (initial) | 0.60 |
| SecYE/SA (final) | 0.71 |
| SecYE/SA (rotated 180°) | 0.41 |
| 1RHZ (SecYE only) | 0.41 |
| 3DIN (SecYE only) | 0.47 |

Supplementary Table 2: Ribosome-SecY interactions

| SecY residue | | Ribosome residue | | Interaction |
|---|---|---|---|---|
| Arg243 | SecY L6/7 | Gln38 | (L29) | H-bond |
| Arg243 | SecY L6/7 | Ura62 | (23S) | hydrophilic |
| Arg243 | SecY L6/7 | Ade63 | (23S) | hydrophilic |
| Val245 | SecY L6/7 | Gua93 | (23S) | H-bond |
| Val246 | SecY L6/7 | Ura62 | (23S) | H-bond |
| Val246 | SecY L6/7 | Ade63 | (23S) | hydrophobic |
| Asn247 | SecY L6/7 | Ade63 | (23S) | H-bond |
| Tyr248 | SecY L6/7 | Lys46 | (L24) | hydrophobic (weak) |
| Tyr248 | SecY L6/7 | Val48 | (L24) | hydrophobic |
| Tyr248 | SecY L6/7 | Ade482 | (23S) | hydrophilic (weak) |
| Arg251 | SecY L6/7 | Ade492 | (23S) | H-bond |
| Arg251 | SecY L6/7 | Gua493 | (23S) | H-bond |
| Gln252 | SecY L6/7 | Ade507 | (23S) | H-bond |
| Gln253 | SecY L6/7 | Gua493 | (23S) | hydrophilic |
| Gln253 | SecY L6/7 | Ade507 | (23S) | H-bond |
| Gln253 | SecY L6/7 | Ade508 | (23S) | hydrophilic |
| Arg255 | SecY L6/7 | Cyt1335 | (23S) | hydrophilic |
| Arg256 | SecY L6/7 | Gln72 | (L23) | H-bond |
| Arg256 | SecY L6/7 | Ade64 | (23S) | H-bond |
| Tyr258 | SecY L6/7 | Cyt1335 | (23S) | H-bond |
| Lys348 | SecY L8/9 | Gua1317 | (23S) | H-bond |
| Lys348 | SecY L8/9 | Ura1318 | (23S) | hydrophilic |
| Phe352 | SecY L8/9 | Cyt1335 | (23S) | H-bond |
| Val353 | SecY L8/9 | Ade1336 | (23S) | H-bond |
| Ile356 | SecY L8/9 | Ura1316 | (23S) | H-bond |
| Ile356 | SecY L8/9 | Gua1337 | (23S) | H-bond |
| Ile356 | SecY L8/9 | Ade1392 | (23S) | hydrophobic |
| Arg357 | SecY L8/9 | Ura1316 | (23S) | H-bond |
| Arg357 | SecY L8/9 | Gua1317 | (23S) | H-bond |
| Arg357 | SecY L8/9 | Ade1392 | (23S) | H-bond |
| Glu360 | SecY L8/9 | Ade1535 | (23S) | H-bond |
| Tyr365 | SecY L8/9 | Asp94 | (L23) | hydrophilic |
| Tyr429 | SecY C-term. | Ala50 | (L24) | hydrophobic |
| Ser431 | SecY C-term. | Cyt490 | (23S) | hydrophilic |
| Lys434 | SecY C-term. | Cyt1320 | (23S) | H-bond |
| Asn437 | SecY C-term. | Cyt1319 | (23S) | H-bond |
| Asn437 | SecY C-term. | Cyt1330 | (23S) | hydrophilic |
| Lys439 | SecY C-term. | Gua1317 | (23S) | hydrophilic |
| Lys439 | SecY C-term. | Ura1318 | (23S) | H-bond |
| Lys439 | SecY C-term. | Gua1331 | (23S) | H-bond |
| Tyr441 | SecY C-term. | Gua1317 | (23S) | H-bond |
| Gly442 | SecY C-term. | Ura1316 | (23S) | H-bond |
| Arg243 | SecY L6/7 | Gln38 | (L29) | H-bond |
| Arg243 | SecY L6/7 | Ura62 | (23S) | hydrophilic |
| Arg243 | SecY L6/7 | Ade63 | (23S) | hydrophilic |
| Val245 | SecY L6/7 | Gua93 | (23S) | H-bond |

Supplementary Table 3: Ribosome-SecE interactions

| SecE residue | | Ribosome residue | | Interaction |
|---|---|---|---|---|
| Arg12 | SecE N-term. | Glu24 | (L29) | H-bond |
| Leu14 | SecE N-term. | Leu37 | (L29) | hydrophobic |
| Glu15 | SecE N-term. | Asn27 | (L29) | hydrophilic |
| Glu15 | SecE N-term. | Gln31 | (L29) | hydrophilic |
| Gly65 | SecE amphi. | Glu100 | (L23) | H-bond |
| Lys66 | SecE amphi. | Glu52 | (L23) | H-bond |
| Lys66 | SecE amphi. | Glu100 | (L23) | H-bond |
| Arg73 | SecE amphi. | Glu89 | (L23) | H-bond/hydrophilic |
| Glu74 | SecE amphi. | Gln91 | (L23) | H-bond |
| Arg76 | SecE amphi. | Phe95 | (L23) | H-bond |
| Thr77 | SecE amphi. | Leu93 | (L23) | H-bond |
| Lys81 | SecE amphi. | Gln36 | (L29) | hydrophilic (weak) |
| Lys81 | SecE amphi. | Asp94 | (L23) | H-bond |
| Trp84 | SecE amphi. | Leu37 | (L29) | hydrophobic |

Supplementary Table 4: NC-ribosome-SecY interactions

| NC residue | | Ribosome/SecY residue | | Interaction |
|---|---|---|---|---|
| Gln104 | NC | Arg84 | (L22) | H-bond |
| Arg102 | NC | Cyt1323 | (23S) | hydrophilic |
| Arg102 | NC | Ade1322 | (23S) | hydrophilic |
| Arg102 | NC | Ade508 | (23S) | hydrophilic |
| Gln101 | NC | Ade1322 | (23S) | H-bond |
| Gln101 | NC | His70 | (L23) | Hydrophilic |
| Glu100 | NC | Ade508 | (23S) | H-bond |
| Glu100 | NC | Gln253 | SecY L6/7 | H-bond |
| Ile99 | NC | Ade1321 | (23S) | hydrophobic |
| Ile99 | NC | Ade1321 | (23S) | H-bond |
| Gln98 | NC | Ade1321 | (23S) | H-bond |
| Gln98 | NC | Ade492 | (23S) | hydrophilic |
| Gln98 | NC | Gua491 | (23S) | H-bond |
| Gln96 | NC | Ade492 | (23S) | H-bond |
| Gln96 | NC | Gua491 | (23S) | H-bond |
| Ile95 | NC | Ala432 | SecY C-term. | hydrophobic |
| Ile94 | NC | Tyr258 | SecY L6/7 | hydrophobic |
| Val92 | NC | Ala432 | SecY C-term. | hydrophobic |
| Val92 | NC | Ala50 | (L24) | hydrophobic |
| Asp91 | NC | Thr263 | SecY L6/7 | hydrophilic (weak) |
| Asp91 | NC | Arg242 | SecY L6/7 | hydrophilic |
| Asp91 | NC | Pro49 | (L24) | H-bond |
| Gln90 | NC | Glu430 | SecY C-term. | hydrophilic |
| Met88 | NC | Pro339 | SecY L8/9 | hydrophobic |
| Met88 | NC | Leu265 | SecY L6/7 | hydrophobic |
| Phe87 | NC | Val274 | SecY TM7 | hydrophobic |
| Phe87 | NC | Asn270 | SecY L6/7 | H-bond |
| Phe87 | NC | Val234 | SecY TM6 | hydrophobic |
| Phe87 | NC | Phe233 | SecY TM6 | hydrophobic |

Supplementary Table 5: NC-SecY interactions

| NC residue | | SecY residue | | Interaction |
|---|---|---|---|---|
| Glu83 | NC | Ile275 | SecY TM7 | H-bond |
| Gly82 | NC | Ile275 | SecY TM7 | H-bond |
| Gly82 | NC | Asn185 | SecY TM5 | H-bond |
| Leu81 | NC | Ile90 | SecY TM2 | hydrophobic |
| Leu81 | NC | Ile275 | SecY TM7 | hydrophobic |
| Leu81 | NC | Ala277 | SecY TM7 | H-bond |
| Leu81 | NC | Pro276 | SecY TM7 | H-bond (weak) |
| Leu81 | NC | Ile86 | SecY TM2 | hydrophobic |
| Ala80 | NC | Ile278 | SecY TM7 | hydrophobic |
| Ala80 | NC | Ile86 | SecY TM2 | H-bond (weak) |
| Ala80 | NC | Ile86 | SecY TM2 | hydrophobic (weak) |
| Ala80 | NC | Ile82 | SecY TM2 | hydrophobic |
| Leu79 | NC | Ile408 | SecY TM10 | hydrophobic |
| Leu79 | NC | Ile278 | SecY TM7 | H-bond (weak) |
| Leu79 | NC | Ile195 | SecY TM5 | hydrophobic |
| Leu79 | NC | Ile191 | SecY TM5 | hydrophobic |
| Leu79 | NC | Tyr85 | SecY TM2 | hydrophobic |
| Leu79 | NC | Ala79 | SecY TM2 | hydrophobic |
| Ile78 | NC | Ile82 | SecY TM2 | hydrophobic |
| Ile78 | NC | Gly81 | SecY TM2 | H-bond |
| Ser77 | NC | Gly81 | SecY TM2 | H-bond (weak) |
| Ser77 | NC | Ile77 | SecY TM2 | H-bond |
| Ser77 | NC | Ser76 | SecY TM2 | H-bond |
| Ser77 | NC | Arg74 | SecY TM2 | H-bond (weak) |
| Gln76 | NC | Gly81 | SecY TM2 | H-bond |
| Gln76 | NC | Arg74 | SecY TM2 | hydrophilic |
| Gln76 | NC | Ser73 | SecY TM2 | hydrophilic |
| Arg75 | NC | Arg74 | SecY TM2 | H-bond (weak) |
| Ile74 | NC | Pro143 | SecY TM3 | hydrophobic |
| Ile74 | NC | Arg74 | SecY TM2 | H-bond |
| Asp73 | NC | Ser76 | SecY TM2 | H-bond |
| Asp73 | NC | Lys51 | SecY TM1 | H-bond |
| Asp72 | NC | Ser76 | SecY TM2 | H-bond (weak) |
| Asn71 | NC | Ile77 | SecY TM2 | H-bond (weak) |
| Asn71 | NC | Gln56 | SecY TM1 | H-bond |

Supplementary Table 6: SA-SecY interactions

| SA residue | | SecY residue | | Interaction |
|---|---|---|---|---|
| Thr23 | SA | Val98 | SecY TM2b | H-bond |
| Thr23 | SA | Val336 | SecY TM8 | H-bond |
| Leu25 | SA | Ile275 | SecY TM7 | hydrophobic |
| Ala26 | SA | Leu94 | SecY TM2b | hydrophobic |
| Ile28 | SA | Phe328 | SecY TM8 | hydrophobic |
| Ile28 | SA | Tyr332 | SecY TM8 | hydrophobic |
| Leu29 | SA | Ile90 | SecY TM2b | hydrophobic |
| Leu29 | SA | Gln93 | SecY TM2b | H-bond |
| Leu29 | SA | Ile275 | SecY TM7 | hydrophobic |
| Phe30 | SA | Met83 | SecY TM2b | hydrophobic |
| Phe30 | SA | Ile86 | SecY TM2b | hydrophobic |
| Phe30 | SA | Ile90 | SecY TM2b | hydrophobic |
| Leu32 | SA | Ile325 | SecY TM8 | hydrophobic |
| Val34 | SA | Ile86 | SecY TM2b | hydrophobic |
| Thr36 | SA | Ser282 | SecY TM7 | H-bond |
| Thr37 | SA | Ile82 | SecY TM2b | H-bond (weak) |
| Leu39 | SA | Ser282 | SecY TM7 | H-bond |
| Leu39 | SA | Phe286 | SecY TM7 | hydrophobic |
| Val40 | SA | Phe64 | SecY TM2 | hydrophobic |
| Val40 | SA | Phe67 | SecY TM2 | hydrophobic |
| Trp43 | SA | Phe64 | SecY TM2 | hydrophobic |
| Trp43 | SA | Phe286 | SecY TM7 | hydrophobic |
| Trp43 | SA | Phe286 | SecY TM7 | H-bond |
| Trp43 | SA | Ile290 | SecY TM7 | hydrophobic |
| Trp43 | SA | Phe294 | SecY TM7 | hydrophobic |
| Val44 | SA | Phe64 | SecY TM2 | hydrophobic |
| Val44 | SA | Gly70 | SecY TM2 | H-bond |
| Val45 | SA | Leu72 | SecY TM2 | hydrophobic (weak) |
| Leu46 | SA | Phe294 | SecY TM7 | hydrophobic |
| Trp48 | SA | Asn65 | SecY TM2 | H-bond |
| Trp48 | SA | Ala71 | SecY TM2 | hydrophobic |
| Trp48 | SA | Ala71 | SecY TM2 | H-bond (weak) |
| Trp48 | SA | Leu72 | SecY TM2 | hydrophobic |
| Met49 | SA | Ile61 | SecY TM2 | hydrophobic |

Supplementary Table 7: Interactions between H59 and lipids

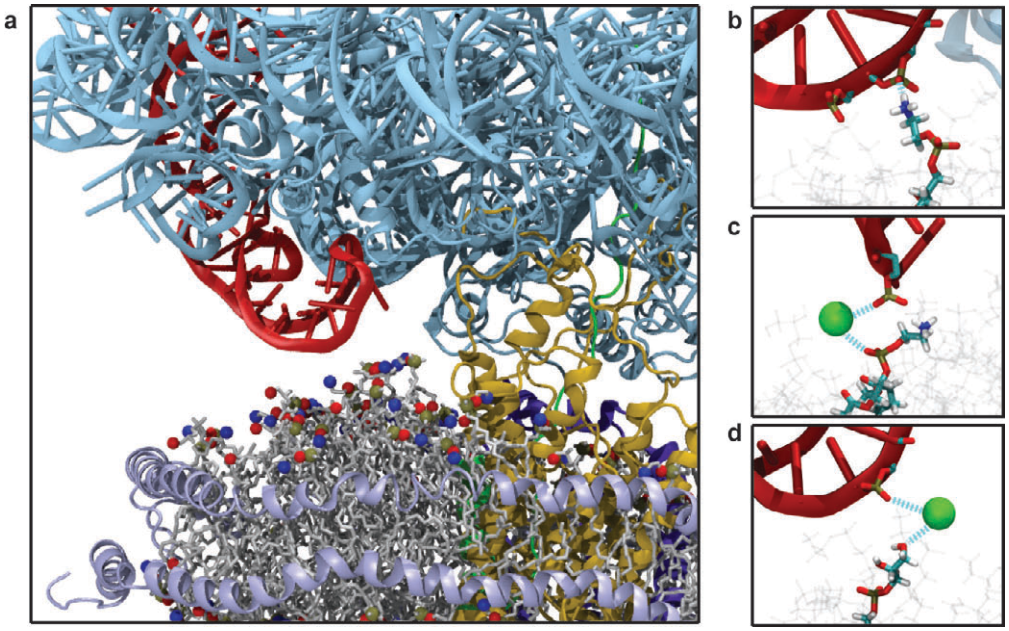


| H59 residue | Lipid Type | Interaction Type | Stable |
|---|---|---|---|
| Cyt1531 | POPE | ion-bridging | no |
| Ade1532 | POPE | ion-bridging | yes |
| Ade1532 | POPE | H-bond | yes |
| Ade1532 | POPG | ion-bridging | yes |
| Cyt1533 | POPE | ion-bridging | yes |
| Cyt1533 | POPE | H-bond | yes |
| Cyt1533 | POPG | ion-bridging | yes |
| Ura1534 | POPE | ion-bridging | yes |
| Ura1534 | POPE | H-bond | yes |
| Ura1534 | POPE | hydrophilic | no |
| Ura1534 | POPG | ion-bridging | no |
| Ade1535 | POPE | ion-bridging | no |
| Cyt1536 | POPE | ion-bridging | no |
| Ura1539 | POPE | ion-bridging | no |
| Gua1540 | POPE | ion-bridging | yes |
| Gua1540 | POPE | H-bond | no |
| Gua1540 | POPG | ion-bridging | no |
| Cyt1541 | POPE | ion-bridging | yes |
| Cyt1541 | POPE | H-bond | yes |
| Cyt1541 | POPG | ion-bridging | no |